Journal of Operation and Automation in Power Engineering

Vol. XX, No. XX, XXXX, Pages: XXXX (Proofed)

http://joape.uma.ac.ir

Research Paper

A Robust Reactive Power Control-Based Protection Paradigm for Large AC Systems with Offshore Wind Turbines

Mahdi Zolfaghari [1, 2, *], *Moslem Salehi* [3], and *Gevork B. Gharehpetian* [2]

[1]*Iran Grid Management Company (IGMC), Tehran, Iran.*
[2]*Department of Electrical Engineering, Amirkabir University of Technology, Tehran, Iran.*
[3]*Department of Electrical Engineering, Technical and Vocational University (TVU), Tehran, Iran.*

Abstract— *The generated electrical power from offshore wind turbines is usually transferred to the main power system through HVDC systems. Nevertheless, if there is a fault at the Point of Common Coupling (PCC) bus of grid-side power converter (GSPC) of the HVDC system, the performance of the distance protection layout of the AC system may be deteriorated because of the fast-dynamic response of the GSPC in reactive power injection into the main AC system. This causes the distance relay to overes-timate the measured impedance, endangering power system security and continuation of supply. Since the GSPC effectively controls the injected reactive power into the AC system, the current paper pro-poses a novel sliding mode control-based scheme for the GSPC to reduce the impact of GSPC action on the performance of the distance relays. The nonlinear dynamics of the GSPC are considered when designing and applying the proposed controller to the GSPC model. The proposed controller is im-plemented in the current control loop of GSPC, facilitating the smooth output current control of GSPC. The main outcome of the proposed paradigm is that the suggested control scheme of GSPC, considers the current flowing through the distance relay. Accordingly, it can appropriately control the output current of the GSPC during a fault. Thus, the action of the GSPC does not affect the distance backup protection. The robustness of the proposed paradigm and proper fast dynamic response of the GSPC, are evaluated in PSCAD/EMTDC.*

Keywords—Distance relaying, sliding mode control, wind turbine, fault detection.

NOMENCLATURE

Abbreviations

DFIG	Doubly-Fed Induction Generator
DSP	Digital Signal Processing
FACTS	Flexible Alternating Current Transmission System
FRT	Fault-Ride-Through
GA	Genetic Algorithm
GSPC	Grid-Side Power Converter
HVDC	High-Voltage Direct Current
KCL	Kirchhoff's Current Law
LL	Line-to-Line Short-Circuit Fault
LLGF	Line-to-Line-to-Ground Short-Circuit Fault
MPPT	Maximum Power Point Tracking
PCC	Point of Common Coupling
PI	Proportional-Integral Controller/Compensator
PSO	Particle Swarm Optimization
PV	Photovoltaic
RES	Renewable Energy Source
SC	Short-Circuit Fault
SCFRZ	Short-Circuit Fault with Fault Resistance Near Zero
SMC	Sliding Mode Control
SVPWM	Space Vector Pulse Width Modulation
UPFC	Unified Power Flow Controller
WSPC	Wind Turbine-Side Power Converter

Received: 25 Jul. 2025
Revised: 26 Nov. 2025
Accepted: 15 Dec. 2025
*Corresponding author:
E-mail: mahdizolfaghari66@gmail.com (M. Zolfaghari)
DOI: 10.22098/joape.2026.17915.2408

1. INTRODUCTION

1.1. Problem description

Renewable energy sources (RESs) and their related problems, such as control and protection, have been a center of main researches during the past two decades [1]. Offshore wind farms are RESs which can provide a significant amount of clean energy [2]. Due to distance constraints, seaward wind turbines are intertied to the primary AC power grid through HVDC frames, as indicated in Fig. 1 [3]. We should recall that HVDC systems can be outlined as monopole or bi-pole configurations. Here, we have considered a monopole structure for faster simulation. As illustrated, the offshore wind systems are integrated and connected to the Bus1, where the wind turbine-side power converter (WSPC) is located [4]. The power-droop control scheme is commonly used to maintain the DC link voltage at the appropriate level [5]. The rectified DC voltage, through the DC side filters and the DC line, is transferred to the DC bus of the GSPC [6]. The GSPC and WSPC operate independently [7]. The GSPC converts the DC voltage to AC voltage with a desired frequency (i.e. 50 Hz or 60 Hz). Accordingly, the GSPC is responsible for AC side voltage and frequency regulation [8]. Further, the active and reactive powers injected to the main AC grid are controlled using the control loops of the GSPC [9]. On the other hand, the AC transmission lines are protected using the distance protection schemes and, in some cases, the operation and fast dynamic response of GSPC in injection of reactive power to the main grid may interfere and disturb the distance protection scheme [10].

In order to understand the problem, consider a portion of main power system in which the HVDC system and the distance relay are involved, as depicted in Fig. 2. The GSPC is connected to PCC through a power transformer. Also, distance Relay 1 is located in far-end side of transmission line 1. The main distance protection scheme is provided by relay 2, located in the transmission line 2. Thus, Zone 2 of Relay 1 acts as a backup for Relay 2. Here, Z_{L1} and Z_{L2} are the impedances of the transmission lines 1 and 2, respectively. Ignoring the current injection by the GSPC into the PCC ($I_{GSPC} = 0$), when a three-phase short circuit fault (SC) occur on line 2, it is expected that the prime protection, i.e. Zone 1 of Relay 2, clear the fault. Otherwise, the backup protection, i.e. Zone 2 of Relay 1, must detect the faults. During the fault conditions, the voltage of the PCC drops and the GSPC reacts to this voltage reduction and injects more reactive power into the PCC to compensate for the inherent voltage drop. This in turn, results in the overestimation of the measured impedance by the distance relay [11]. Thus, a Zone 2 SC fault condition might not be detected and cleared within the critical clearing time and this endangers the power system security and stability. Therefore, appropriate control of the GSPC is essential considering the requirements of the protection schemes for removing faults at the expected clearing time limits [12].

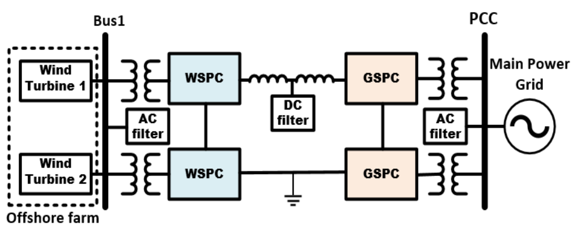

Fig. 1. A seaward wind turbine connected to the primary power network through a HVDC system.

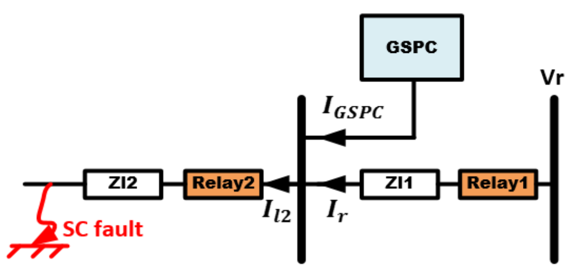

Fig. 2. A part of power system with a HVDC system and a distance protection scheme.

1.2. Literature review

For resolving the conflict raised from the fast reactive power control of GSPC and the distance pro-tection scheme, the techniques presented in the literature can be classified into two general groups:1) the techniques which propose adaptive settings for distance protection schemes, and 2) the techniques which offer control actions for RESs or GSPC to prevent distance protection malfunctions. At rest, some of these techniques for each group are reviewed. The authors in [13] have presented a protection strategy based on providing adaptive settings for distance relays. The method is based on calculation of network impedance matrix in which the system impedances are continually calculated and sent for the distance protection schemes. However, the al-gorithm is time consuming and the control of the GSPC has been unmanipulated. In [14], a twenty-layer artificial neural network has been proposed to enhance the performance of distance protection schemes in the presence of RESs. The proposed technique has been capable of correctly classifying the fault types and fault locations to reduce distance relay malfunction. The author in [15] has presented an in-telligent distance protection using a modified version of differential evolution algorithm. The technique has used performance engineering to achieve appropriate results for the distance scheme performance. Considering a modular multilevel converter based HVDC system, the researchers in [16] have discussed the system power angle on the characteristics of distance protection. The model of asymmetrical LLG fault has been analyzed considering the effects of zero sequence of fault current. The results indicate that the zero-sequence component had an important effect on fault detection when modular multilevel converters are used. In [17], using electromagnetic simulations, it is shown that the inverter-based re-sources have an important effects on the performance of distance relays and especially, the asymmetrical faults such as LLG, may deteriorate the correct functioning of distance schemes. In [18], an impedance calculation method has been proposed for distance relays in the presence of RESs. The method has been able to detect the correct fault impedance and locate it in the defined boundaries. The authors in [19] have analyzed the fault records in a real offshore windfarm system with Siemens Energy Company. It is concluded that the zero-sequence path has an important effect on the functioning of the distance pro-tection scheme. In [20] an artificial neural network-based distance protection scheme has been reported. The method considers the windfarm output fluctuations and dynamically changes the reference im-pedance of the distance relay.

Some distance protection schemes presented in the literature have analyzed the characteristics of FACTS equipment on the distance protection systems. The main focus of these approaches is on the readjustment of Zone 2 of the backup relay and not on the control of GSPC. For example, in [21] the effects of static VAr compensators on the operation of distance scheme have been analyzed. The authors have investigated the differential protection of a wind turbine in a modular multi-level converter-based HVDC (MMC-HVDC) system. It is indicated that the phase difference, which the relay is operated based on, should be remained in a defined range to bring an effective protection performance. To pro-vide this requirement, it is proposed to align the phase angle of the fault current with the angle of the output current of the wind turbine. Accordingly, a coordinated control scheme for MMC has been proposed to align the phase angles. In [22] a power system containing a UPFC and distance relays has been studied. The operational effects of UPFC on the system impedance have been verified and an adaptive distance protection strategy has been presented.

In [23], the effects of control systems of power converters of HVDC systems of offshore wind farms on the different protection schemes of the power system, including overcurrent relays, distance relay, and differential relay have been investigated. For this purpose, firstly the characteristics of highly con-trolled fault current has been analyzed. Secondly, various study cases have been defined and analyzed in order to characterize the response of fault current of the HVDC-connected offshore wind farm. The authors in [24] have studied the impact of other RESs, mainly the large PVs, on the distance protection schemes. It is indicated that output variation of the PV systems can affect the performance of distance relays. To resolve the problem, the authors have not used commonly used mho or quadrilateral char-acteristics. Instead, they have claimed a method based on equivalent network model which is inde-pendent from the output characteristics and parameters of the PV system. Nevertheless, the proposed protection scheme is based on the positive-sequence network model. In [25], it is shown that the par-ticipation of the converter-driven resources, mainly the wind turbines and PVs, in short circuit current fault in a converter-based power system should be limited because of the low overcurrent capacity of semi-conductors of the power converters. Through semi-actual simulation tests, it is indicated that the control systems of power converters can have considerable effect on the performance of the distance relays. The investigated results show that the constant reactive power control scheme can deteriorate the performance of the protection scheme while constant active power control or balanced current control scheme can improve the fault detection schemes. The researches in [26] have set-up a model suitable for investigating the effects of renewable source on the performance of distance protection schemes. It is accentuated that the grid codes have enforced the RESs to bring-up the fault ride-through (FRT) ca-pability to interact with power systems in fault conditions. Nevertheless, the malfunctioning of distance protections may counterpoise the FRT capability of the RESs by detecting an out-of-zone fault as an in-zone fault and vice versa. To investigate this problem, it is indicated that a suitable model should be attained for the researchers in order to analyze and compare the results. Thus, the proposed model has been verified as a proper workbench for such studies. Following the clues given by [26], the authors in [27] have proposed a time delay and zero-sequence impedance-based protection scheme in order to resolve the problem of interfering the renewables with the distance protection scheme. The method has its pros and cons. Nevertheless, the model described by [26] has been implemented on a real-time digital simulator and the simulations studies have been done based on this model.

Furthermore, a short circuit fault has been set in field test in an actual power plant to verify the proposed control structure. Both the real-time simulation and field test results have confirmed the properness of the protection model. Later on, the same authors in [28] proposed a cosine similarity index-based fault detection methods through processing of features of faults signals. In [29], it is indicated that the wind farms connected to the power systems can mainly affect the differential protection schemes and constant threshold set point are not useful when there are wind turbines integrated with power grids. Accordingly, fault signals have been processed for detecting modulations based on particle swarm optimization (PSO) algorithm. Using the positive sequence system model, unbalanced fault model is considered for the analysis. The method has been able to calculate the threshold of distance protection scheme in order to cope with the FRT re-quirements of grid codes. The method considers the location and beginning angle as the objective function for the optimization process. In [30], a combination of distance and differential relays has been proposed to set up the protection scheme of a grid-connected doubly-fed induction generator (DFIG). Instead of making the boundaries of the relay adaptive with variations of wind speed, the technique has used the calculation of active power at both ends of the protected transmission line. Then, the fault resistance and therefore the fault location are calculated. Further in [31], it is indicated that the capacitive current of long transmission lines, which connects a large-scale wind turbines to the main power grid, can deviate the protection scheme of the line. Accordingly, instead of using magnitude of current, the signs of samples of currents have been used in the protection scheme. Also, an adaptive online calcu-lation method for obtaining the relay settings has been recommended.

Recently, the sliding mode controllers (SMC) have been used in many power system applications. For example, in [32], the SMC controller has been considered to adjust the output voltage of a PV system which is operating in islanding mode. In the studied system, the load demonstrates a variable con-sumption pattern. In such a condition, the proposed SMC controller preserves the output voltage of the DC/DC converter at a constant level. In [33], a set of parallel-connected PV systems has been consid-ered where the main purpose was to develop an appropriate power sharing among PVs. The PV systems have been equipped with a new SMC-based maximum power point tracking (MPPT) system. It has been shown that the proposed SMC-based structure was able to withstand against changes in system condition and show the best performance. In [34], considering a stepwise approach, a SMC has been designed for an islanded power inverter. In order to reduce the chattering problem, the researchers in [35] have proposed an adaptive PI controller in a SMC structure used for a robot manipulator. Further in [36], a SMC scheme has been developed for multilevel power converters in order to reduce the circu-lating current and improve the voltage regulation and power balance. Table 1 summarizes the literature review.

1.3. Objectives and contributions

The basic objective of this paper is to prompt a control strategy for GSPC considering the current flowing through the backup distance relay. The purpose of this strategy is that the distance protection scheme is not affected by GSPC interference. The proposed scheme provides more degrees of freedom and this allows for the distance relays to become more accurate in estimating the impedance. The proposed controller, which is designed based on the sliding mode concept, is more applicable to the current control loop of the GSPC since it considers the nonlinear dynamics of the GSPC in the design process. Thus, the design of nonlinear controller for the purpose of preserving the distance protection scheme from HVDC converters is the research gap covered by this study.

Accordingly, the main contributions of this paper are as follows:

- A new control scheme for GSPC of HVDC with the purpose of preserving distance backup protection is outlined based on sliding mode concept.
- The nonlinear dynamics of the GSPC are considered when designing and applying the controller to the GSPC model. This makes the application of the proposed controller in the current control loop of GSPC, facilitating the smooth output current control of GSPC with the purpose of appropriate performance of the distance backup protection.

1.4. Paper organization

The paper is outlined as follows: Section 2 presents the proposed protection scheme and the design process of the sliding mode-based controller. The simulation results and comparison case studies are showcased in Section 3. Finally, Section 4 concludes the study.

2. Sliding Mode Control-based Distance Protection Paradigm

2.1. Proposed strategy

The outline of the proposed strategy is indicated in Fig. 3. As shown, a sliding mode-based scheme is adapted to control the GSPC. The feedback currents and references are fed to the sliding mode controller to minimize the errors. According to Fig. 3, if $I_{GSPC} = 0$, the impedance observed at Relay 1 (i.e., Z_{R1}), is:

$$Z_{R1} = Z_{l1} + Z_{l2} \tag{1}$$

when $I_{GSPC} \neq 0$,

$$Z_{R1} = Z_{l1} + Z_{l2}\left(\frac{I_{\text{GSPC}} + I_r}{I_r}\right) \tag{2}$$

by defining the current ratio as follows:

$$K = \frac{I_{\text{GSPC}}}{I_r} \tag{3}$$

then, Eq. (2) transforms to:

Table 1. Classification of some literature studies in this field.

Objective of study	Reference No.	Problem resolving strategy
Preserving the performance of distance protection schemes in HVDC-integrated power grids	[5], [13], [18], [20], [23], [31]	Adapting settings for distance relays
	[4], [30], [37]	Modifying control systems of HVDC converters
Preserving the performance of over-current/differential/distance relays in the presence of RESs	[24], [28], [29]	Using adaptive control schemes or robust control theory

$$Z_{R1} = Z_{l1} + (K+1)Z_{l2} \tag{4}$$

These impedances result from the transmission lines resistances and inductances. Note that Eq. (4) shows that when $I_{GSPC} \neq 0$, the recognized impedance through Relay 1 is a function of current ratio K. Therefore, changing K may result in overestimation or underestimation of the recognized impedance seen by the distance relay. To overcome this shortcoming, we propose forcing the current ratio near a steady-state value to insure the stability of the measured impedance. Using KCL at the point of Relay 2:

$$I_{\mathrm{GSPC}} = (K-1)I_r \tag{5}$$

transforming Eq. (5) to alpha-beta reference gives:

$$I^{\alpha}_{\mathrm{GSPC}} = (K^{\alpha}-1)\,I^{\alpha}_r - K^{\beta} I^{\beta}_r \tag{6}$$

$$I^{\beta}_{\mathrm{GSPC}} = (K^{\alpha}-1)\,I^{\beta}_r + K^{\beta} I^{\alpha}_r \tag{7}$$

with

$$I^{(\alpha,*)}_{\mathrm{GSPC}} = \left(K^{(\alpha,*)}-1\right) I^{\alpha}_r - K^{(\beta,*)} I^{\beta}_r \tag{8}$$

$$I^{(\beta,*)}_{\mathrm{GSPC}} = \left(K^{(\alpha,*)}-1\right) I^{\beta}_r + K^{(\beta,*)} I^{\alpha}_r \tag{9}$$

where $\mathrm{I}^{\alpha,*}_{\mathrm{GSPC}}$ and $\mathrm{I}^{\beta,*}_{\mathrm{GSPC}}$ are reference values for a given parameter K. The value of K is chosen based on the value of the injected power of GSPC into the main power grid, i.e. the ratio of the apparent power of the GSPC to the VA of the transmission line on which the relay is installed. Under normal circumstances, K is kept near unity to make the viewed impedance approximately constant. The alpha-beta components of the GSPC current are compared to their references and the observed errors are fed to the sliding mode controller. The sliding mode controller attempts to minimize these errors. Since the voltage at the GSPC is governed by the reactive power injection, the proposed control scheme attempts to minimize changes in the GSPC reactive power simultaneously as when a SC fault occurs. Therefore, the active and reactive powers are given as follows:

$$P_{\mathrm{GSPC}} = \frac{3}{2}\left(V^{\alpha}_{\mathrm{GSPC}} I^{(\alpha,*)}_{\mathrm{GSPC}} + V^{\beta}_{\mathrm{GSPC}} I^{(\beta,*)}_{\mathrm{GSPC}}\right) \tag{10}$$

$$Q_{\mathrm{GSPC}} = \frac{3}{2}\left(V^{\alpha}_{\mathrm{GSPC}} I^{(\beta,*)}_{\mathrm{GSPC}} + V^{\beta}_{\mathrm{GSPC}} I^{(\alpha,*)}_{\mathrm{GSPC}}\right) \tag{11}$$

The detailed diagram of the suggested SMC-based control strategy for the GSPC is illustrated in Fig. 4. As shown, the reference current ratio and the GSPC currents are calculated and fed to the SMC con-troller to calculate the voltage reference signals. The space vector PWM (SVPWM) module uses these references to generate the switching signal which is utilized by the GSPC. It should be noted that the current ratio is a function of current flowing through Relay 1. Therefore, it is a time-varying parameter and may deteriorate the closed-loop system performance. However, the proposed SMC-based controller makes the closed-loop system robustly stable because the time-varying uncertainties have been included in the design process, as described in the following subsection.

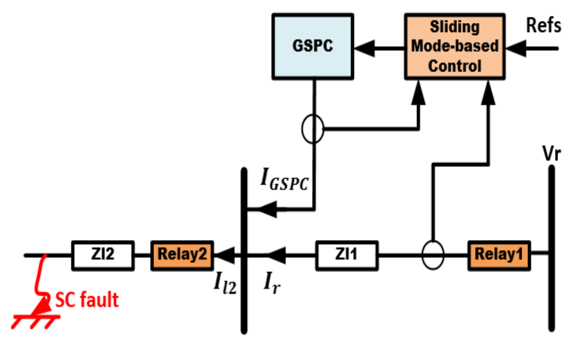

Fig. 3. Overall diagram of the suggested strategy.

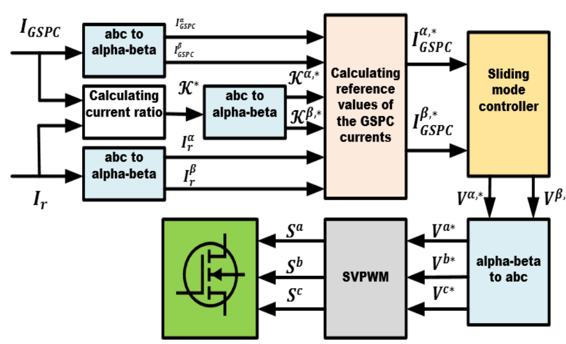

Fig. 4. Proposed SMC-based control of GSPC.

2.2. Designing the SMC-based controller

Considering the output filter, and applying the $\alpha\beta$-transform to the three-phase circuit of the GSPC we have:

$$V^{\alpha}_{\mathrm{GSPC}} = I^{\alpha}_{\mathrm{GSPC}} R_l + L_l \frac{dI^{\alpha}_{\mathrm{GSPC}}}{dt} + V^{\alpha} \tag{12}$$

$$V^{\beta}_{\mathrm{GSPC}} = I^{\beta}_{\mathrm{GSPC}} R_l + L_l \frac{dI^{\beta}_{\mathrm{GSPC}}}{dt} + V^{\beta} \tag{13}$$

where R_l and L_l are, respectively, resistance and inductance of the transmission line which connects the HVDC systems to the main power system. Errors are defined as follows:

$$e^{\alpha}(t) = I_{\text{GSPC}}^{(\alpha,*)} - I_{\text{GSPC}}^{\alpha} \tag{14}$$

$$e^{\beta}(t) = I_{\text{GSPC}}^{(\beta,*)} - I_{\text{GSPC}}^{\beta} \tag{15}$$

The purpose of the SMC strategy is to force the GSPC to track the predefined current trajectories in the $\alpha\beta$ reference frame based on the following sliding (switching) surfaces:

$$\partial^{\alpha}(t) = e^{\alpha}(t) + K^{\alpha}\int_0^t e^{\alpha}(\tau)\,d\tau - e^{\alpha}(0) \tag{16}$$

$$\partial^{\beta}(t) = e^{\beta}(t) + K^{\beta}\int_0^t e^{\beta}(\tau)\,d\tau - e^{\beta}(0) \tag{17}$$

where K^{α} and K^{β} are positive constants. Note that SMC is designed in such a way to operate the system on a particular surface known as a sliding surface. On this sliding surface, defined here as Eqs. (16) and (17), the system always behaves in the desired manner. Once the operational state is achieved, the SMC keeps the operating point in the vicinity of the sliding surface through the control law. Thus, here, when the system states reach the sliding surface, the current components are equal to their related references:

$$\partial^{\alpha}(t) = \partial^{\beta}(t) = 0 \tag{18}$$

$$\dot{\partial}^{\alpha}(t) = \dot{\partial}^{\beta}(t) = 0 \tag{19}$$

Therefore,

$$\dot{e}^{\alpha}(t) = -K^{\alpha}e^{\alpha}(t) \tag{20}$$

$$\dot{e}^{\beta}(t) = -K^{\beta}e^{\beta}(t) \tag{21}$$

Obtaining the derivative of Eqs. (16) and (17) generates:

$$\dot{\partial}^{\alpha}(t) = \frac{d}{dt}\left(I_{\text{GSPC}}^{(\alpha,*)} - I_{\text{GSPC}}^{\alpha}\right) + K^{\alpha}\left(I_{\text{GSPC}}^{(\alpha,*)} - I_{\text{GSPC}}^{\alpha}\right) \tag{22}$$

$$\dot{\partial}^{\beta}(t) = \frac{d}{dt}\left(I_{\text{GSPC}}^{(\beta,*)} - I_{\text{GSPC}}^{\beta}\right) + K^{\beta}\left(I_{\text{GSPC}}^{(\beta,*)} - I_{\text{GSPC}}^{\beta}\right) \tag{23}$$

Defining $\partial(t) = \begin{bmatrix} \partial^{\alpha}(t) \\ \partial^{\beta}(t) \end{bmatrix} = \partial^{\alpha\beta}(t)$, $\dot{\partial}(t) = \begin{bmatrix} \dot{\partial}^{\alpha}(t) \\ \dot{\partial}^{\beta}(t) \end{bmatrix} = \dot{\partial}^{\alpha\beta}(t)$ with the use of Eqs. (7), (8), and (12) and (13) we get:

$$\dot{\partial}^{\alpha\beta}(t) = -\tfrac{1}{L_l}\left(V_{\text{GSPC}}^{\alpha\beta} - V^{\alpha\beta} - I_{\text{GSPC}}^{\alpha\beta}R_l\right) + K^{\alpha\beta}\left(I_{\text{GSPC}}^{(\alpha\beta,*)} - I_{\text{GSPC}}^{\alpha\beta}\right) \tag{24}$$

or alternatively:

$$\dot{\partial}^{\alpha\beta}(t) = G + \frac{1}{L_l}V^{\alpha\beta} \tag{25}$$

where

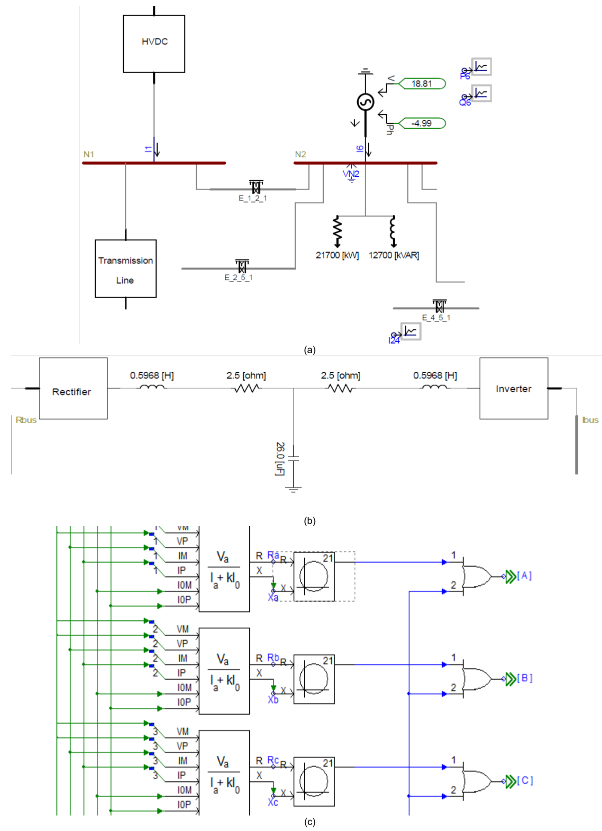

Fig. 5. Simulated model in PSCAD: (a) an offshore wind unit is connected to the IEEE 14-bus standard model, (b) the HVDC system with grid-side and wind-side converters (GSPC and WSPC), and (c) a part of the implemented distance logic.

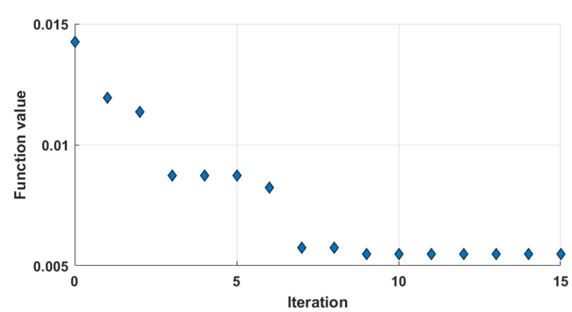

Fig. 6. Cost function of tuning PI parameters.

$$G = -\tfrac{1}{L_l}\left(V_{\text{GSPC}}^{\alpha\beta} - I_{\text{GSPC}}^{\alpha\beta}R_l\right) + K^{\alpha\beta}\left(I_{\text{GSPC}}^{(\alpha\beta,*)} - I_{\text{GSPC}}^{\alpha\beta}\right) \tag{26}$$

To make the system robustly stable and enforcing the system states to reach the sliding manifold, a Lyapunov function is implemented as follows:

$$W = \frac{1}{2}\partial(t)\,\partial^{T}(t) \geq 0 \tag{27}$$

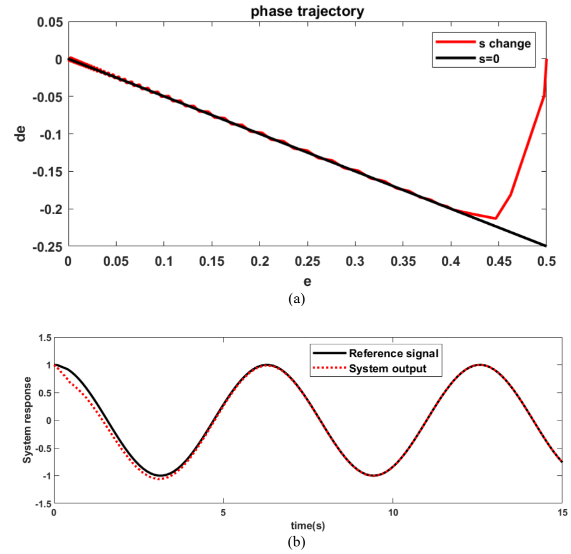

Fig. 7. The performance of the designed SMC scheme: (a) phase trajectory, and (b) tracking error.

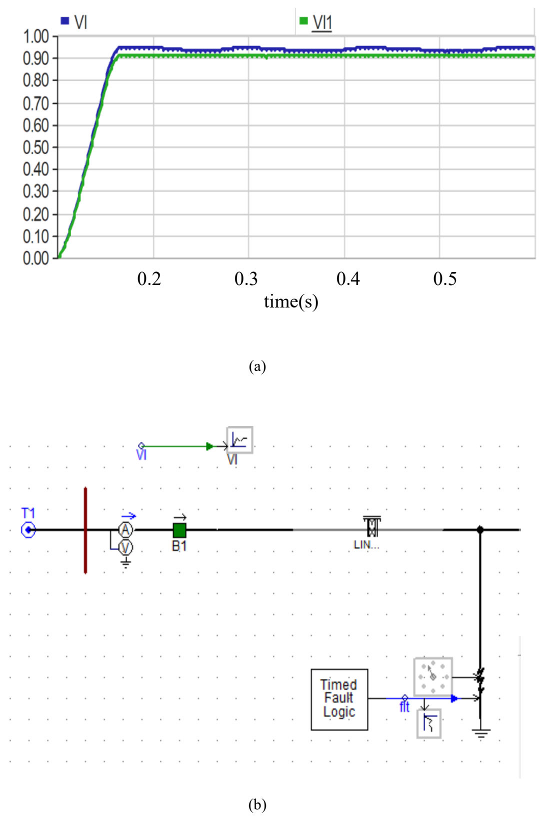

Fig. 8. Voltage (in p.u.) at terminals of the GSPC for a SCFRZ: (a) Vl: when the traditional GSPC control system is used, and Vl1: when the proposed reactive power control system is applied, and (b) the point at which the voltage is measured.

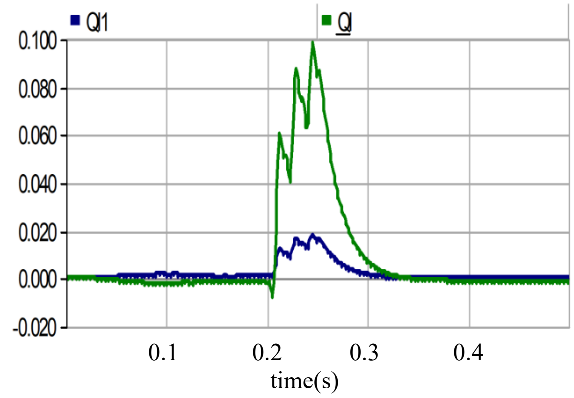

Fig. 9. Reactive power (in p.u.) of the GSPC for a SCFRZ: Ql: when the traditional GSPC control system is used, and Ql1: when the proposed reactive power control system is applied.

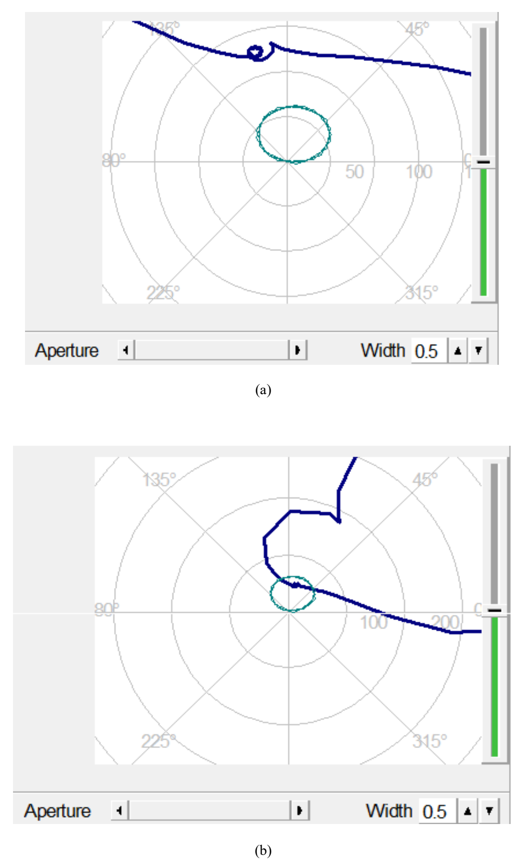

Fig. 10. PSCAD output curve graph: defined boundaries of Zone 2 of the relay and impedance of the system for a SCFRZ: (a) with traditional control of GSPC, and (b) with proposed control of GSPC.

$$\dot{W} = \tfrac{1}{2}\partial^T(t)\dot{\partial}(t) + \tfrac{1}{2}\partial(t)\dot{\partial}^T(t) = \partial^T(t)\left(G + \tfrac{1}{L_l}V^{\alpha\beta}\right) \tag{28}$$

Note that the designed Lyapunov function permit to realize the finite-time stability analysis in control systems with switching structure controllers. The control law is chosen so that the selected Lyapunov function Eq. (27) is negative and $\partial(t) \neq 0$. Therefore, the control law is chosen as follows:

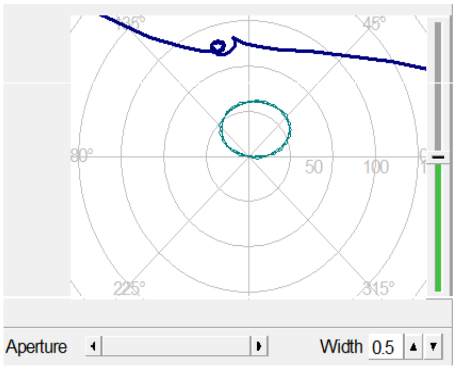

(a)

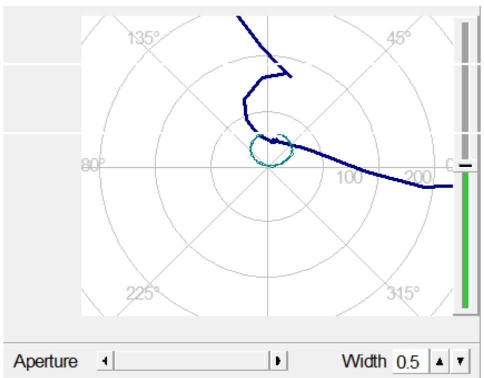

(b)

Fig. 11. PSCAD output curve graph: defined boundaries and impedance of the system for a LLGF: (a) with traditional control of GSPC, and (b) with proposed control of GSPC.

$$V^{\alpha\beta} = -L_l\left(\begin{bmatrix} G_\alpha \\ G_\beta \end{bmatrix} + \begin{bmatrix} K^{1\alpha} & 0 \\ 0 & K^{1\beta} \end{bmatrix}\begin{bmatrix} \mathrm{sgn}(\partial^\alpha(t)) \\ \mathrm{sgn}(\partial^\beta(t)) \end{bmatrix}\right) \tag{29}$$

where $K^{1\alpha}$ and $K^{1\beta}$ are positive control gains and $sgn(.)$ is the sign function. Substituting Eq. (29) into (28) gives:

$$\dot{W} = \partial^T(t)\dot{\partial}(t) = -\partial^T(t)\begin{bmatrix} K^{1\alpha} & 0 \\ 0 & K^{1\beta} \end{bmatrix}\begin{bmatrix} \mathrm{sgn}(\partial^\alpha(t)) \\ \mathrm{sgn}(\partial^\beta(t)) \end{bmatrix} < 0 \tag{30}$$

Thus, the time-derivative of the Lyapunov function is negative and the system is stable. The numerical solution for $K^{1\alpha}$ and $K^{1\beta}$ are approximately 4.8 and 3.2, respectively. For more details on solving Lyapunov equations, see [38].

3. Simulation Results

The performance of the suggested robust reactive power control-based protection scheme is evaluated here through simulations study cases in PSCAD. It is expected that the performance of the fault detection (via the distance relays) is not deteriorated by the operation of the power converters of the HVDC system, especially when equipped with the GSPC with the proposed control structure as illustrated in Fig. 4. To demonstrate this, two study cases are considered using the IEEE 14-bus system standard benchmark. The offshore wind unit which is connected to the main grid through an HVDC system, is demonstrated in Fig. 5-(a). The parameters of the wind turbine, distance characteristics, controller gains, and simulation settings are given in Table 2. The IEEE 14-bus test system data are given in Tables 3 and 4 in the Appendix. The conventional current control scheme, which uses PI controllers to control the GSPC, is considered for comparison purposes here. For the base case, the PI parameters have optimally been tuned using the GA algorithm in MATLAB to have the best performance. The optimal values of the controller parameters are $K_P = 3.2$ and $K_I = 5.7$. The cost function of tuning process is illustrated in Fig. 6. We have also analyzed the stochastic behavior of wind turbines when evaluating the performance of the PI-based and the suggested robust control-based protection paradigm. The phase trajectory of the proposed SMC scheme and the tracking error are shown in Fig. 7. These results show more than 98% accuracy in reference tracking. The response of the conventional and the proposed control schemes to a three-phase SC fault with fault resistance near zero (SCFRZ) is studied in Case 1. The responses of the two studied control schemes to an asymmetrical fault (LLG fault) is analyzed in Case 2. Notice that the direct LL fault is not analyzed here because its verification and response is almost similar to the SCFRZ fault. The series impedance of lines is implemented as $Z_{line} = 1.79 + j17 = 17.093\angle 83.98\ \Omega$. The fault duration is 100 ms in all cases and fault location is at 50% of length of the transmission line.

Table 2. Reproducibility parameters.

Parameter	Value
Parameters of simulated offshore wind system	
Nominal power	2×3 MW
Density of air	1.2 $\mathrm{kg/m^3}$
Initial wind speed	13 m/s
Cut-in speed	3 m/s
Cut-off speed	25 m/s
Pitch angle (max)	25°
Rate of change of pitch angle (max)	2°/s
Generator type	DFIG
Nominal generator voltage	0.69 kV
Generator stator resistance	0.01 p.u.
Generator stator reactance	0.1 p.u.
Distance relay characteristic coordinates	
Coordinates of the centre as (x, y)	0
Radius of the circle (r_d)	32
X-coordinate of the centre (x_1)	5.5
Y-coordinate of the centre (y_1)	31.5
Z-coordinate of the centre (Z)	1
Controller gains	
K^1_α	4.8
K^1_β	3.2
Theta coordinate of the centre (θ)	1.48353 rad
Simulation settings	
Duration of run (s)	0.6
Solution time step (μs)	10
Channel plot step (μs)	100
Duration of fault (ms)	100
Fault location (from far-end bus)	50% of line length

It should be noted that for real case implementation of the proposed strategy, a digital signal processing (DSP) platform or an Opal-RT system is needed for real time simulations. Using the new power electronics boards with fast switching frequency capability, the implementation of the proposed control structure can be applied to the real GSPCs in power systems.

3.1. Three-phase direct SC fault

For the sake of comparison, we firstly consider a common current control method for the GSPC. Then, in a similar operation condition, we apply the proposed scheme to the GSPC. A faulty system condition is simulated in which a SCFRZ fault take places at the tail-end of ZONE 2 of the installed relay device, i.e., half the distance of line number 2 to which the GSPC of HVDC structure is intertied. At t = 0.2s a SCFRZ fault occurs and sustains for 7 cycles, (or 116.67 ms) Figs. 8-10 demonstrate the results during the defined condition. As shown in Fig. 8, the output voltage of the HVDC system at the point of connection undergoes changes for both the common current controller and the suggested controller. As shown, when we adopt the common current controller, the output voltage of GSPC has a small voltage drop. The reason for this small drop is that the common current control method uses the traditional PI compensators which have fast response but poor dynamic tuning capabilities. The response of the GSPC with the suggested control structure is also shown in Fig. 8. As can be seen, the output voltage of the GSPC has a smaller drop, distortion and overshoot/undershoot, lower than 5% in comparison with the PI controller. The result shows enhanced dynamic performance in the term of removing the negative transient portion in the waveform. As shown in Fig. 9, when the SCFRZ fault initiates at t = 0.2s, the output voltage of the GSPC begins to decrease, and thus, the control loops of the GSPC react to the voltage drop by reducing the amount of consumed reactive power in order to retrieve the voltage at the GSPC terminals. As shown, the traditional scheme reacts as fast as possible to the voltage drop in the terminals of the GSPC to compensate for the voltage drop, the control system attempts to reduce the reactive power injected by the GSPC. This fast reduction of reactive power results in an erroneous estimation of the impedance seen by the relay. Nevertheless, by adopting the proposed control system for the GSPC, the controller does not force the GSPC to reduce the injection of reactive power as much as the traditional control system does. Ultimately, the reactive power is more stable when implementing the proposed reactive power control scheme. Accordingly, as shown in Fig. 10, implementing the proposed control scheme results in allotment of the impedance path inside Zone 2 of the relay. Since the main objective of the proposed reactive control method is to regulate the current ratio near a steady-state value, therefore, the impedance is kept to the desired trajectory. According to Fig. 10, when utilizing the traditional control method for GSPC, the impedance observed by the relay does not reside within Zone 2. The amplitude of the observed impedance is around 20.391 Ω which is larger than 17.093 Ω. Nevertheless, when the proposed reactive power control scheme is utilized for the GSPC, the amplitude of the impedance observed by the relay becomes roughly 17 Ω which closely follows the system impedance 17.093 Ω. Accordingly, the impedance observed in Zone 2 of the relay is resided within the defined boundaries.

3.2. Line-to-line-to-ground SC fault

To further examine the performance of the proposed reactive power control of GSPC, we consider a line-to-line-to-ground SC fault (LLGF) with fault resistance of 10 Ω. The duration and clearing instant of the fault are kept identical to those used in previous subsection. Fig. 11 illustrates the impedance allocation graph of Zone 2 of the relay. As shown, when using the traditional method, the output impedance is nearly the same as previous subsection. This is due to the fact that the behavior of the traditional control does not change with the fault type and characteristics. The real value of the system impedance (amplitude) including the LLGF resistance is roughly 20.71 Ω. Based on the results demonstrated in Fig. 11, when the traditional control method is used for GSPC, the impedance amplitude seen by relay 21.92 Ω. Nevertheless, by adopting the proposed reactive power control scheme, the impedance amplitude is about 20.542 Ω. Hence, the application of the proposed reactive power control scheme results in more accurate impedance value seen by Zone 2 of the relay which reside within defined boundaries.

4. CONCLUSION

This work proposes an approach for the optimal scheduling of distributed generators (DGs) in a microgrid that includes residential, industrial, and commercial voltage-dependent loads, which fluctuate across different seasons. The Shuffled BAT Optimization Algorithm (SBOA) is utilized to establish the most efficient schedules, aiming to minimize losses, voltage variations, and generating costs. This approach ensures reliable load fulfillment, as measured by the reliability index EIR. The approach is evaluated on the modified 33-bus radial distribution system, considered as an MMG system with three microgrids. Additionally, the influence of demand response (DR) initiatives on optimal day-ahead scheduling in a microgrid with various renewable energy sources (RES) is investigated. Three DR-based scenarios—without DRPs, with Time-of-Use (TOU) pricing, and with Real-Time Pricing (RTP)—are studied. In the case without DRP, based on the Mean, the cost function optimized with PSO achieves a better global optimum value of about $1974.07/hr. Compared to stochastic optimization, PSO yields a global optimum value and reduces the price reduction by 1.05%. With DRPs, based on the standard deviation, the optimal value of the cost function was obtained using PSO and stochastic optimization as $73.45/hr and $96.17/hr for TOU, respectively. Comparing PSO with stochastic optimization for TOU based on standard deviation, PSO achieves a better price reduction of 30.5% than stochastic optimization. For RTP, based on standard deviation, PSO demonstrates better optimal performance, with a 15.9% improvement over stochastic optimization. The results illustrate the significant benefits of DRPs in multi-microgrids, particularly in reducing costs for both power suppliers and consumers by flattening the demand curve. The Particle Swarm Optimization (PSO) algorithm effectively addresses the issues of optimal microgrid scheduling, even with uncertain parameters, proving its advantages over stochastic optimization methods. Furthermore, the Jaya algorithm, a novel metaheuristic optimization technique, is employed to optimize single and multi-objective functions, such as lowering operational expenses, system losses, and voltage deviations, on a modified 33-bus distribution system. The results obtained using the Jaya algorithm are compared with those obtained using the Genetic Algorithm (GA), showing an operational cost of about $178,158.36/hr, power losses of 56.15 kW, and voltage deviations of 1.05E-03. Comparing these results with GA, the superiority of the Jaya algorithm is evident, as it achieves minimal operating costs, system losses, and voltage deviations. The Jaya algorithm reduces the operational cost of the multi-microgrid by about 16.4% compared to GA, with power losses being 20.7% lower than GA.

The proposed strategy can result in inaccurate load predictions, which may lead to inefficient scheduling, potentially increasing operating expenses or compromising system reliability. Due to uncertainties, robust optimization methods are required, which add complexity to the task. As the number of microgrids and distributed generation systems (DGs) increases, the optimization model becomes more complex and more challenging to solve. Many algorithms face challenges in achieving efficient scalability, which limits their application in large-scale MMG systems.

To address these issues, future work should explore hybrid methodologies that integrate heuristic techniques, such as greedy algorithms, with metaheuristics, such as genetic algorithms, to achieve a balance between solution quality and computational efficiency. These approaches could be customized to provide faster convergence while still obtaining solutions that are close to optimal. For load forecasting, stochastic optimization methods that consider uncertainty in both renewable generation and load estimates should be utilized. These techniques can improve scheduling efficiency in various scenarios, enhancing resilience to unexpected changes.

ACKNOWLEDGEMENT

The authors acknowledge the use of artificial intelligence tools (e.g., ChatGPT by OpenAI) for language editing and clarity improvement during the preparation of this manuscript. The authors are fully responsible for the scientific content, analysis, and conclusions.

References

[1] S. Biswas and B. K. Panigrahi, "An improved fault detection and phase identification for collector system of dfig-wind farms using least square transient detector coefficient," *Electr. Power Syst. Res.*, vol. 226, p. 109961, 2024.

[2] N. Kumar and D. K. Jain, "Development of an adaptive protection scheme for microgrid operation suitable for grid-connected and Islanded mode," *J. Oper. Autom. Power Eng.*, vol. 13, no. 4, pp. 255–268, 2025.

[3] N. Bagheri, B. Tousi, and S. M. Alilou, "A topology of non-isolated soft switched DC-DC converter for renewable energy applications," *J. Oper. Autom. Power Eng.*, vol. 13, no. 4, pp. 294–302, 2025.

[4] M. N. Uddin, N. Rezaei, and M. S. Arifin, "Hybrid machine learning-based intelligent distance protection and control schemes with fault and zonal classification capabilities for grid-connected wind farms," *IEEE Trans. Ind. Appl.*, vol. 59, no. 6, pp. 7328–7340, 2023.

[5] L. He, C. C. Liu, A. Pitto, and D. Cirio, "Distance protection of AC grid with HVDC-Connected offshore wind generators," *IEEE Trans. Power Del.*, vol. 29, no. 2, pp. 493–501, 2014.

[6] A. A. R. Mohamed, H. M. Sharaf, and D. K. Ibrahim, "Enhancing distance protection of long transmission lines compensated with tcsc and connected with wind power," *IEEE Access*, vol. 9, pp. 46717–46730, 2021.

[7] M. N. Uddin, M. S. Arifin, and N. Rezaei, "A novel neuro-fuzzy based direct power control of a DFIG based wind farm incorporated with distance protection scheme and LVRT capability," *IEEE Trans. Ind. Appl.*, vol. 59, no. 5, pp. 5792–5803, 2023.

[8] S. K. Gupta and S. K. Mallik, "Voltage stability assessment of power system using line indices with wind system and solar photovoltaic generation integration," *J. Oper. Autom. Power Eng.*, vol. 13, no. 4, pp. 303–314, 2025.

[9] R. Bekhradian, A. Mahari, M. Abedini, and M. Sanaye-Pasand, "Innovative probabilistic approach to reduce zone-2 time delay setting of distance relays," *Electr. Power Syst. Res.*, vol. 229, p. 110116, 2024.

[10] A. K. Pradhan and G. Joos, "Adaptive distance relay setting for lines connecting wind farms," *IEEE Trans. Energy Convers.*, vol. 22, no. 1, pp. 206–213, 2007.

[11] A. Jodaei and Z. Moravej, "Fault detection and location in power systems with large-scale photovoltaic power plant by adaptive distance relays," *Iran. J. Energy Environ.*, vol. 15, no. 3, pp. 265–278, 2024.

[12] M. Zolfaghari, G. B. Gharehpetian, and M. Abedi, "A repetitive control-based approach for power sharing among boost converters in DC microgrids," *J. Oper. Autom. Power Eng.*, vol. 7, no. 2, pp. 168–175, 2019.

[13] T. S. Sidhu, R. K. Varma, P. K. Gangadharan, F. A. Albasri, and G. R. Ortiz, "Performance of distance relays on shunt-FACTS compensated transmission lines," *IEEE Trans. Power Del.*, vol. 20, no. 3, pp. 1837–1845, 2005.

[14] A. N. Sheta, A. A. Eladl, B. E. Sedhom, M. I. El-Afifi, P. Sanjeevikumar, and M. Zaki, "Artificial neural network-based enhanced distance protection sensitivity in microgrids," *Renew. Energy Focus*, vol. 54, p. 100710, 2025.

[15] J. F. Piñeros, "Intelligent model to automatically determine and verify distance relays settings," *Electr. Power Syst. Res.*, vol. 217, p. 109137, 2023.

[16] Z. Zhou, S. Yu, X. Wang, H. Cao, Q. Cheng, and J. Liu, "The impact of system power angle on power frequency variation distance protection of AC transmission lines connected to the receiving end converter of MMC-HVDC system," in *Proc. IEEE 2nd Int. Conf. Power Sci. Technol.*, pp. 326–331, 2024.

[17] M. Saifussalam, F. S. Rahman, and N. Hariyanto, "Distance protection performance of transmission lines influenced by inverter-based resources," in *Proc. 6th Int. Conf. Power Eng. Renew. Energy*, pp. 1–6, 2024.

[18] H. Ma, Z. Chen, X. Fu, T. Zhang, and T. Zheng, "An asymmetric fault distance protection method for inverter-interfaced renewable energy transmission lines," in *Proc. 3rd Asia Power Electr. Technol. Conf.*, pp. 90–94, 2024.

[19] T. Waugh, F. Song, and R. Leone, "Application of distance protection to offshore windfarm with external disturbance," in *Proc. 17th Int. Conf. Dev. Power Syst. Prot.*, vol. 2024, pp. 343–348, 2024.

[20] H. Sadeghi, "A novel method for adaptive distance protection of transmission line connected to wind farms," *Int. J. Electr. Power Energy Syst.*, vol. 43, no. 1, pp. 1376–1382, 2012.

[21] G. Gao, H. Wu, F. Blaabjerg, and X. Wang, "Fault current control of MMC in hvdc-connected offshore wind farm: A coordinated perspective with current differential protection," *Int. J. Electr. Power Energy Syst.*, vol. 148, p. 108952, 2023.

[22] Z. Xiaoyao, W. Haifeng, R. K. Aggarwal, and P. Beaumont, "Performance evaluation of a distance relay as applied to a transmission system with UPFC," *IEEE Trans. Power Del.*, vol. 21, no. 3, pp. 1137–1147, 2006.

[23] G. Gao, H. Wu, and X. Wang, "Converter control impacts on efficacy of protection relays in HVDC-Connected offshore wind farms," in *Proc. IEEE 13th Int. Symp. Power Electron. Distrib. Gener. Syst.*, pp. 1–6, 2022.

[24] A. Ghorbani and H. Mehrjerdi, "Distance protection with fault resistance compensation for lines connected to PV plant," *Int. J. Electr. Power Energy Syst.*, vol. 148, p. 108976, 2023.

[25] J. Jia, G. Yang, A. H. Nielsen, and P. Rønne-Hansen, "Impact of VSC control strategies and incorporation of synchronous condensers on distance protection under unbalanced faults," *IEEE Trans. Ind. Electron.*, vol. 66, no. 2, pp. 1108–1118, 2019.

[26] A. Hooshyar, M. A. Azzouz, and E. F. El-Saadany, "Distance protection of lines emanating from full-scale converter-interfaced renewable energy power plants—part I: Problem statement," *IEEE Trans. Power Del.*, vol. 30, no. 4, pp. 1770–1780, 2015.

[27] Y. Fang, K. Jia, Z. Yang, Y. Li, and T. Bi, "Impact of inverter-interfaced renewable energy generators on distance protection and an improved scheme," *IEEE Trans. Ind. Electron.*, vol. 66, no. 9, pp. 7078–7088, 2019.

[28] L. Zheng, K. Jia, T. Bi, Y. Fang, and Z. Yang, "Cosine similarity based line protection for large-scale wind farms," *IEEE Trans. Ind. Electron.*, vol. 68, no. 7, pp. 5990–5999, 2021.

[29] C. D. Prasad, M. Biswal, and A. Y. Abdelaziz, "Adaptive differential protection scheme for wind farm integrated power network," *Electr. Power Syst. Res.*, vol. 187, p. 106452, 2020.

[30] A. Ghorbani, H. Mehrjerdi, and N. A. Al-Emadi, "Distance-differential protection of transmission lines connected to wind farms," *Int. J. Electr. Power Energy Syst.*, vol. 89, pp. 11–18, 2017.

[31] A. Saber, M. F. Shaaban, and H. H. Zeineldin, "A new differential protection algorithm for transmission lines connected to large-scale wind farms," *Int. J. Electr. Power Energy Syst.*, vol. 141, p. 108220, 2022.

[32] M. Zolfaghari, A. Zolfaghari, G. B. Gharehpetian, R. Ahmadiahangar, and A. Rosin, "Output voltage regulation of isolated PV-Connected boost converters with variable loads using converted hysteresis sliding mode controller," in *Proc. IEEE 17th Int. Conf. Compat., Power Electron. Power Eng.*, pp. 1–7, 2023.

[33] M. Zolfaghari, S. H. Hosseinian, S. H. Fathi, M. Abedi, and G. B. Gharehpetian, "A new power management scheme for parallel-connected PV systems in microgrids," *IEEE Trans. Sustain. Energy*, vol. 9, no. 4, pp. 1605–1617, 2018.

[34] M. Barzegar-Kalashani, M. A. Mahmud, B. Tousi, and M. Farhadi-Kangarlu, "A step-by-step full-order sliding mode controller design for standalone inverter-interfaced cleaner

renewable energy sources," *Cleaner Energy Syst.*, vol. 6, p. 100080, 2023.

[35] S. Khorashadizadeh and M. M. Fateh, "Adaptive fourier series-based control of electrically driven robot manipulators," in *Proc. 3rd Int. Conf. Control, Instrum. Autom.*, pp. 213–218, 2013.

[36] M. Aghahadi, L. Piegari, A. Lekić, and A. Shetgaonkar, "Sliding mode control of the MMC-based power system," in *Proc. IECON 2022 – 48th Annu. Conf. IEEE Ind. Electron. Soc.*, pp. 1–6, 2022.

[37] M. Zolfaghari, R. M. Chabanlo, M. Abedi, and M. Shahidehpour, "A robust distance protection approach for bulk AC power system considering the effects of HVDC interfaced offshore wind units," *IEEE Syst. J.*, vol. 12, no. 4, pp. 3786–3795, 2018.

[38] E. Jarlebring, "Numerical methods for Lyapunov equations." Lecture Notes in Numerical Linear Algebra, KTH University, 2017.

APPENDIX

IEEE 14-bus test system data

Table 3. Voltage conditions for initialization.

Bus	V **(kV)**	δ **(deg)**	P **(p.u.)**	Q **(p.u.)**
1	146.28	0.0000	2.3239	−0.1655
2	144.21	−4.9826	0.4000	0.4356
3	139.38	−12.7250	0.0000	0.2508
6	147.66	−14.2209	0.0000	0.1273
8	150.42	−13.3596	0.0000	0.1762

Table 4. Line impedance and susceptance.

Line		R **(p.u./m)**	X **(p.u./m)**	B **(p.u./m)**
From Bus	**To Bus**			
1	2	1.94E−07	5.92E−07	5.28E−07
1	5	5.40E−07	2.23E−06	4.92E−07
2	3	4.70E−07	1.98E−06	4.38E−07
2	4	5.81E−07	1.76E−06	3.40E−07
2	5	5.70E−07	1.74E−06	3.46E−07
3	4	6.70E−07	1.71E−06	1.28E−07
4	5	1.34E−07	4.21E−07	1.00E−09
6	11	9.50E−07	1.99E−06	1.00E−09
6	12	1.23E−06	2.56E−06	1.00E−09
6	13	6.62E−07	1.30E−06	1.00E−09
7	8	1.00E−09	1.76E−06	1.00E−09
7	9	1.00E−09	1.10E−06	1.00E−09
9	10	3.18E−07	8.45E−07	1.00E−09
9	14	1.27E−06	2.70E−06	1.00E−09
10	11	8.21E−07	1.92E−06	1.00E−09
12	13	2.21E−06	2.00E−06	1.00E−09
13	14	1.71E−06	3.48E−06	1.00E−09